Editors' Suggestion

Nonlinear terahertz transmission spectroscopy on Ga-doped germanium in high magnetic fields

Bence Bernáth,[1,2,*] Papori Gogoi,[1,2] Andrea Marchese,[1,2] Dmytro Kamenskyi,[1,2,3,4,†] Hans Engelkamp,[1,2] Denis Arslanov,[2,3] Britta Redlich,[2,3] Peter C. M. Christianen,[1,2] and Jan C. Maan[1,2,3]

[1]*High Field Magnet Laboratory (HFML-EMFL), Radboud University, Toernooiveld 7, 6525 ED Nijmegen, The Netherlands*

[2]*Radboud University, Institute for Molecules and Materials, Heyendaalseweg 135, 6525 AJ Nijmegen, The Netherlands*

[3]*FELIX Laboratory, Radboud University, 6525 ED Nijmegen, The Netherlands*

[4]*Experimental Physics V, Center for Electronic Correlations and Magnetism, Institute of Physics, University of Augsburg, 86159 Augsburg, Germany*

(Received 11 March 2022; revised 2 May 2022; accepted 4 May 2022; published 18 May 2022)

We report the observation of cyclotron resonance (CR) transitions of holes in the magnetotransmission spectra of gallium-doped germanium at low temperatures, using intense, pulsed THz free-electron laser radiation with a photon energy lower than the ionization energy of the Ga dopants (11 meV). The THz radiation, in the range of 12–89 cm^{-1}, both creates free holes through photoionization of Ga and induces the CR of these holes. For photon energies above the lowest energy internal Ga transition (55 cm^{-1}), intradopant transitions are simultaneously observed with narrow CR peaks. For energies below 55 cm^{-1}, with increasing THz radiation intensity first the lowest Landau level transitions of all heavy-hole and light-hole subbands appear. This marks the onset of photoionization, which is found to be more efficient for lower laser frequencies, consistent with field-ionization (Keldysh parameter $<< 1$). For the highest laser intensities, the CR peaks of the heavy (light) holes shift to higher (lower) magnetic field, as a result of the increasing population of the higher-energy nonequidistant Landau levels, consistent with the effective-mass theory of the hole subbands in Ge.

DOI: 10.1103/PhysRevB.105.205204

I. INTRODUCTION

The development of high-intensity THz free-electron lasers (FELs) has enabled the investigation of nonlinear phenomena in semiconductors and low-dimensional materials in the THz regime. Important examples are multiphoton absorption [1,2], photoionization [3–5], absorbance saturation [6–10], ultrafast inter(sub)band carrier dynamics, and multiple ways of coherent control [11–14]. To expand their potential, FELs are combined with high magnetic fields in some laboratories around the world. These combination facilities have been used to study pulsed electron paramagnetic resonance [15,16], magnetic resonances [17–19], dynamics of charge carriers in Landau levels (LLs) [6,20–22], and bound states of dopant atoms [9].

Here, we use a THz FEL in combination with a 33 T Florida-Bitter magnet to investigate photoionization and cyclotron resonance (CR) in gallium-doped germanium (Ge:Ga) over a wide range of THz intensities. Nonlinear processes in hole-doped germanium (*p*-Ge) have been investigated to advance the development of lasers [23,24] and THz technology [25–28]. Despite the fact that *p*-Ge has been widely studied, also in high magnetic fields [29–31], several outstanding issues still remain, which are mostly related to the nonparabolic band structure of the valence band, the appearance of nonequidistant LLs [32–34], and the lack of a clear understanding of the light-induced ionization of the dopant atoms [35–39]. Figure 1 shows schematically the band structure of Ge:Ga near the bottom of the valence band. The ionization energy (E_i) of Ga in Ge is 11 meV, which is equivalent to 128 K or 89 cm^{-1}, meaning that at liquid helium temperatures the amount of free holes in the band is negligible. Low-intensity THz spectroscopy at low temperatures will therefore detect only intracenter transitions, the lowest of which are labeled by C, D, and G. Free holes can be created in a number of ways, such as raising the temperature, the application of an external electric field, or by optical excitation using incident radiation with an energy near the band gap of the material (creating electron-hole pairs) or the ionization energy of the dopant atom (creating only free holes) [35]. In addition, as we will show below, free carriers can also be created through light-induced ionization of the dopant atoms, using light with an energy below the ionization energy [40].

The complex subband structure has resulted in the experimental observation of very interesting features in the CR spectrum of *p*-Ge [29]. The results depend strongly on how many LLs (counted by index n) are occupied, what light frequency and intensity is used, and at which temperature T and magnetic field strength B the study is executed. To classify whether or not specific quantum effects in the CR spectra are present, the quantum effect parameter $\eta = \frac{\hbar\omega}{k_B T}$ is introduced, where $\hbar\omega$ is the photon energy of the radiation used, and $k_B T$ is the thermal energy. In the first experiments, at high temperatures and/or at low magnetic fields, quantum effects were not recognized [40,41]. Two hole bands—light hole (LH) and heavy hole (HH)—were reported with effective masses of $m^*_{LH} = 0.04 m_e$ and $m^*_{HH} = 0.3 m_e$ (m_e is the free-electron mass), and no sign of absorption saturation was

*Corresponding author: benceahaver@gmail.com

†Present address: Institute of Optical Sensor Systems, German Aerospace Center (DLR), 12489 Berlin, Germany; dmytro.kamenskyi@dlr.de

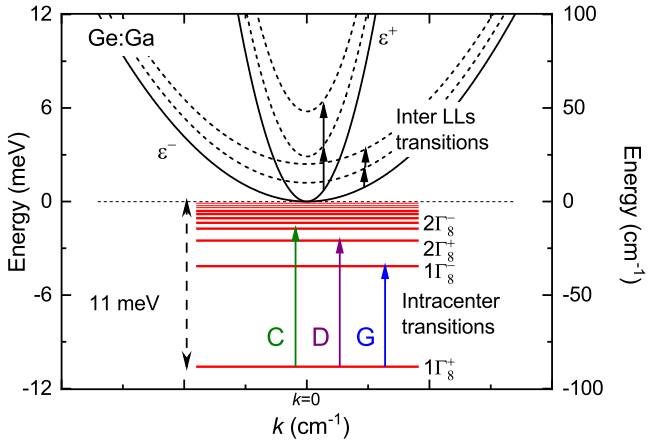

FIG. 1. Schematic representation of the valence-band energy levels in Ge:Ga. Zero energy is defined at the bottom of the valence band. The red solid lines indicate the Ga levels; the vertical colored arrows show the lowest three intracenter transitions, labeled by C, D, and G. The vertical dashed arrow shows the spacing between the Ga ground state and the bottom of the valence band at zero magnetic field (11 meV, corresponding to the ionization energy). The solid black lines correspond to the heavy-hole (ϵ^-) and light-hole (ϵ^+) subbands, and the dashed black lines indicate their LLs when a magnetic field is applied. The vertical black solid arrows indicate the cyclotron resonance transitions in between the LLs.

observed. These masses are correct, but later on it turned out that they originate from higher-energy LLs (with high n number), for which the effective mass is different from that associated with the states at lower energy and low n-values. These first studies were performed in the temperature range of 1.3–4.2 K using continuous wave (CW) microwave sources (9–25 GHz) and above-band-gap white tungsten light to create free carriers [42]. In other words, η was small, between 0.11 and 0.29, so only two distinct hole peaks were observable. Under these conditions, the population of the high-index LLs is high, and details of the complex band structure at the band edge are not observable.

Later on, using high-frequency radiation and $\eta > 1$, quantum effects became visible in p-Ge [30,42,43]. A summary of these experiments is discussed in Ref. [29], revealing very rich spectra with many absorption peaks, identifying up to five different transitions with masses between $0.044m_e$ and $0.256m_e$. There is a tendency that with larger resonance energy ($\hbar\omega$), the observed effective mass m^* is larger, which can be attributed to the interaction of the valence band with the conduction and split-off bands [29]. Although an intense THz laser has been used for CR studies of p-Ge [43], to the best of our knowledge there is no systematic study of the intensity dependence of the CR transitions in p-Ge.

In our study, η was much larger than 1 (between 4.3 and 91.4). We found that the intense THz light simultaneously creates free holes through photoionization and induces inter-LL transitions. We first characterized the p-Ge samples in the low excitation limit by using the low-intensity THz light of a Fourier transform infrared (FTIR) spectrometer. This resulted in an overview of the energy positions of the intracenter Ga transitions as a function of magnetic field (measured at 1.3 K) and the positions of the lowest energy CR transitions (measured at 20 K). For the FEL experiments, we used a photon energy range of 1.5–11 meV (12–89 cm^{-1}), which means that we were able to study the laser frequency dependence on the onset of the THz photoionization and to distinguish different regimes. First, we investigated a low photon energy regime of the ionization (below the lowest level labeled $1\Gamma_8^-$ at 6.8 meV equivalent to 55 cm^{-1}). And second, we studied the ionization assisted by intracenter transitions when the photon energy is larger than 6.8 meV. For FEL photon energies above 6.8 meV, we saw both intracenter and CR transitions, where the latter dominate at higher FEL intensities. For energies below 6.8 meV, we observed multiple CR transitions, with positions and amplitudes that depend strongly on the FEL intensity, as a result of the saturation of some CR transitions and an increasing occupation of higher-energy LLs, both with increasing FEL radiation intensity. Using the same light source for both free-carrier creation and inducing CR transitions is usually avoided because under these circumstances it is difficult to keep the carrier concentration constant, which makes the interpretation of the CR line shapes difficult [35,44]. However, our method has a big advantage. We are able to populate higher-energy LLs while keeping the lattice temperature low. As a result, CR transitions for high index LLs appear, and the CR positions shift with increasing THz intensity. We compare our results with the theory of the germanium valence band [34].

II. EXPERIMENTS

A. Experimental instruments and sample

Two setups were used for our experiments. Low-power, frequency-resolved far-infrared spectra were measured at fixed magnetic fields, using an FTIR spectrometer (Bruker IFS113V) connected to a 33 T Florida-Bitter magnet [45]. The interferograms were detected by a silicon bolometer nearby the sample. Each transmission interferogram was Fourier-transformed, then each spectrum was corrected with the same, calculated common background. This background spectrum was calculated from all spectra at all magnetic fields by taking for each frequency the 90th percentile [46] intensity value. With this normalization method, the water lines and other field-independent features were removed. For the final figures, we inverted these normalized spectra.

For the high-power THz measurements, we used a setup that combines a 33 T Florida-Bitter magnet and the free-electron laser FLARE (Free electron Laser for Advanced spectroscopy and high Resolution Experiments), which covers a broad THz frequency range (7–100 cm^{-1}/0.2–3 THz) [17]. The FLARE light consists of macro- and micropulses. The macropulses are 10 μs long, have a repetition rate of 5 Hz, and consist of a series of micropulses with a repetition rate of either 60 MHz or 3 GHz, depending on the operation mode used. Each micropulse contains approximately 40 optical cycles under a Gaussian envelope. In the 60 MHz mode, the micropulses are well-separated in time, whereas in the 3 GHz mode the micropulses overlap in time, which affects the spectral width of the radiation. Within the 3 GHz mode, depending on the FEL cavity alignment [17], the spectral resolution is about $\frac{\Delta\nu}{\nu} = 0.1\%$, whereas the 60 MHz mode

exhibits a spectral width of about $\frac{\Delta\nu}{\nu} = 1\%$. The spacing of the micropulses (i.e., different spectral bandwidths of the two modes) affects the dynamical properties of the holes, as we will discuss later.

Below 36 cm^{-1}, an InSb hot electron bolometer (QMC Instruments) was used, whereas above this frequency a gallium-doped germanium photoconductive detector (in-house development) was used. We recorded every single macropulse and used a digital boxcar averager on the detector signal.

We used two *p*-type gallium-doped samples, cut from two different, 500 micron thick, germanium wafers (obtained from MTI Corporation) with the same nominal room-temperature resistivity value (10–15 Ω cm). From this resistivity, we estimated the doping concentration to be (2.11–3.18) × 10^{14} cm^{-3} [47]. The top surface of the wafers corresponds to the (100) crystal plane. One sample was used for the experiments with the FTIR and the 3 GHz mode of FLARE. This sample was 2° wedged to avoid Fabry-Pérot interference between their front and back surfaces. The other sample (not wedged) was used for the experiments using the 60 MHz mode of FLARE. For each experiment, the sample was glued on a 5-mm-diameter aperture using GE Varnish. A 5-mm-diameter cone was mounted 3 mm above the sample to focus the light. The sample was mounted in the center of a Florida-Bitter magnet [45] within a liquid-helium bath cryostat, using helium exchange gas to cool the sample. The magnetic field and the $\vec{k}$ vector of the light were oriented along the (100) axis of the crystal (Faraday configuration) in all measurements. Regarding the sample holder and its surroundings, there is no difference between the FEL-based and FTIR spectrometer.

We used 15 different frequencies of FLARE, and at each frequency we used at least two different laser intensities. The raw and processed data of all the measurements are posted in the data repository of the Supplemental Material [48].

B. Low-intensity FTIR measurements

Figure 2 shows the low-power transmission spectra of Ge:Ga obtained in magnetic fields up to 28 T at 1.3 K. At this temperature, the number of free holes in the valence band is low. No LL transitions are observed, and all transmission peaks originate from internal transitions between Ga levels. Without an applied magnetic field, the peaks are positioned at 55 cm^{-1} (G), 69 cm^{-1} (D), and 74 cm^{-1} (C), corresponding to the transitions from the $1\Gamma_8^+$ ground state to the $1\Gamma_8^-$, $2\Gamma_8^+$, and $2\Gamma_8^-$ states, respectively [49]. Each of these states is fourfold degenerate and split in magnetic field due to the Zeeman effect (colored dashed lines in Fig. 2 are guides for the eye). The observed Zeeman splittings of the Ga states in Ge exhibit both linear and quadratic Zeeman terms, similar to the earlier reported behavior of boron dopants in Ge [50].

Figure 3 shows the transmission spectra at an elevated temperature of 20 K. At this temperature, free holes are present in the valence band, resulting in the observation of a set of five relatively broad transmission peaks, four of which correspond to inter-LL transitions (following the notation of Ref. [32]) in the ϵ_2^+, ϵ_1^+ (LHs) and ϵ_1^-, ϵ_2^- (HHs) subbands (indicated by the dashed lines in Fig. 3). The origin of the fifth transition line (pink line) will be discussed later on. However, the relatively large width of the CR peaks in this high-temperature FTIR study hampers a thorough analysis. Figure 4 summarizes the peak positions of all observed transitions, distinguishing the intracenter Ga transitions (purple circles) and the inter-LL CR

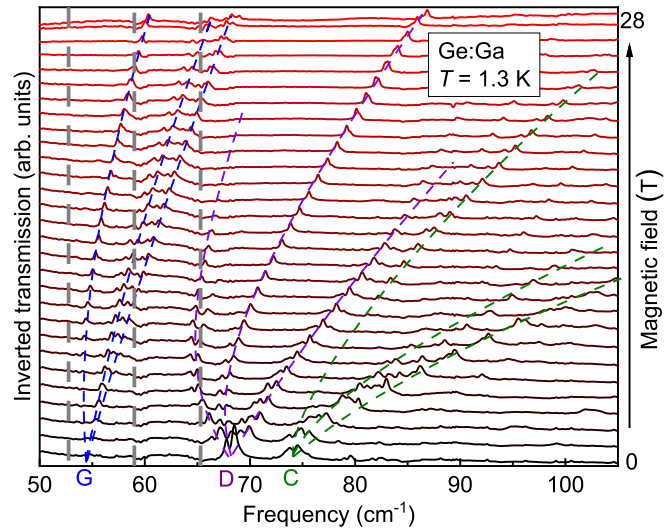

FIG. 2. Inverted FTIR transmission spectra of Ge:Ga at 1.3 K in applied magnetic fields up to 28 T. G, E, and D label the lowest energy Ga intracenter transitions (see Fig. 1). The dashed colored lines are guides to the eye, illustrating how the transitions split in magnetic fields. Each spectrum has been vertically offset corresponding to the applied magnetic field (1 T steps). The three vertical gray dashed lines label the frequencies used in the FEL low-intensity experiments reported in Fig. 5.

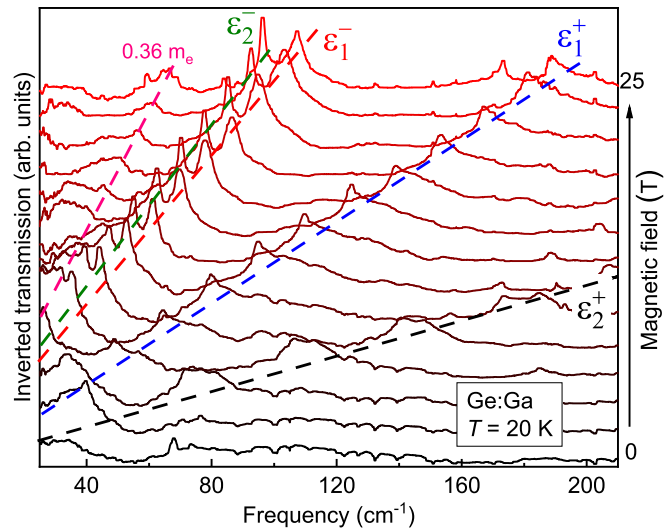

FIG. 3. Inverted FTIR transmission spectra of Ge:Ga at 20 K in applied magnetic fields up to 25 T. The dashed lines indicate the field dependence of the CR transitions for the ϵ_2^+, ϵ_1^+, ϵ_1^-, ϵ_2^- subbands. The pink dashed line indicates a hole CR transition characterized by an effective mass of $0.36m_e$ hole, which was reported earlier but the origin of which is still unknown [33]. The small sharp peaks correspond to water lines. Each spectrum has been vertically offset corresponding to the applied magnetic field (2 T steps).

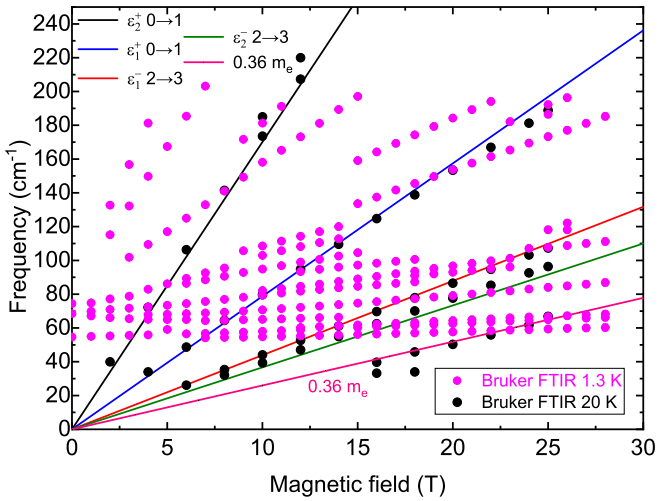

FIG. 4. Peak positions of all transitions detected in the low-intensity FTIR measurements. The purple (black) dots report the results of the 1.3 K (20 K) measurements. The solid lines display the calculated positions of the lowest-energy LL transitions at zero momentum for the ϵ_2^+, ϵ_1^+, ϵ_1^-, ϵ_2^- subbands, using the theory of Evtuhov [34]. The pink line indicates a CR transition involving a hole with an effective mass of $0.36m_e$, which was reported earlier but the origin of which is still unknown [33].

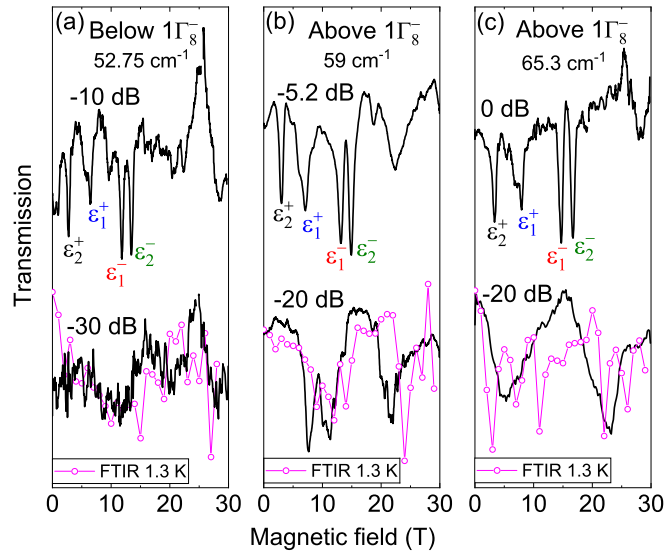

FIG. 5. Comparison of the FTIR and FEL measurements at low intensities (bottom curves) and FEL experiments at higher intensities (top curves). Black lines correspond to FEL spectra obtained using the 3 GHz mode, whereas magenta curves + symbols show the discrete FTIR traces. The high-power FEL spectra are chosen to express the highest contrast from the low-power measurements. The frequencies and the 0 dB intensities are (a) 52.75 cm^{-1} and 320.74 W/cm^2, (b) 59 cm^{-1} and 100.81 W/cm^2, and (c) 65.3 cm^{-1} and 78.51 W/cm^2.

transitions (black circles) with a linear field dependence (the solid lines correspond to the calculated lowest LL transitions, following the theory of Evtuhov [34].

C. High-intensity THz FEL measurements

In our high-intensity FEL-based experiments in the frequency range of 12.9–89 cm^{-1}, we distinguish two different regimes for frequencies below and above the G transition at 55 cm^{-1}. Above 55 cm^{-1}, we expect both internal transitions in the Ga dopants as well as the CR of holes at high excitation intensities, whereas below 55 cm^{-1}, only CR transitions can be excited. The bottom curves in Fig. 5 compare FTIR (magenta curves) and FEL (black curves) experiments for the different regimes (52.75, 59, and 65.3 cm^{-1}) in the low-intensity limit using the 3 GHz mode. It is important to note that even though both measurements are in the low-power regime, there is a difference in intensity of many orders of magnitude. To compare those signals, we have removed the background of the FTIR data and have normalized all the curves, following a procedure that is discussed in the Supplemental Material [48].

Indeed, the low intensity 52.75 cm^{-1} traces [Fig. 5(a)] are basically featureless, whereas the 59 and 65.3 cm^{-1} traces [Figs. 5(b) and 5(c)] exhibit the main interlevel transitions. The minima of the FTIR data reveal the intracenter Ga transitions (along the gray vertical dashed lines in Fig. 2). The low-intensity FEL curves roughly coincide with the FTIR data, within the error of the measurements [51]. The high-intensity FEL data (top curves of Fig. 5) display a completely different behavior. The intracenter Ga transitions are not visible anymore, because they are saturated by the intense FEL light. Instead, very sharp peaks are visible for all frequencies, which can be attributed to CR transitions of the holes occupying the subbands $\epsilon_{1,2}^{+,-}$. These results unambiguously demonstrate that high-power THz radiation with energies below E_i is able to create free carriers through photoionization and, simultaneously, excite inter-LL transitions. Microwave-induced ionization of dopants in Ge was reported previously [35,36,40], but the simultaneous observation of impurity transitions with CRs has not been reported yet. In the Supplemental Material [48] we give more details about the coexistence of the two different kinds of transitions. Note that at low lattice temperature, the LL transitions are quite narrow, which allows a thorough analysis of the peak positions versus magnetic field strength and FEL intensity. Figure 6 shows the evolution of the transmission spectra with power for the FEL frequencies 14.5, 23, and 31.5 cm^{-1} (all below the internal Ga transitions), measured using the 60 MHz mode. At low intensities the curves are featureless, because the FEL frequency is below the lowest intracenter Ga transition and because no free holes are present. With increasing power, sharp CR peaks appear, indicating that also under these conditions the FEL light simultaneously creates free holes through nonresonant photoionization and induces transitions between the hole LLs. At low fields, the CR transitions of the ϵ_2^+, ϵ_1^+ subbands are very pronounced, whereas at higher fields heavy-hole CR peaks appear, albeit that the individual HH levels ($\epsilon_{1,2}^-$) cannot be resolved due to the small splitting at this low field/frequency, leading to one relatively broad transmission dip, marked as HHs. Clearly, the relative amplitudes of the different CR transitions depend strongly on the FEL intensity. For instance, the 14.5 cm^{-1} data show that with increasing FEL intensity, ϵ_1^+ and ϵ_2^+ become more clear but finally saturate. The HH peak

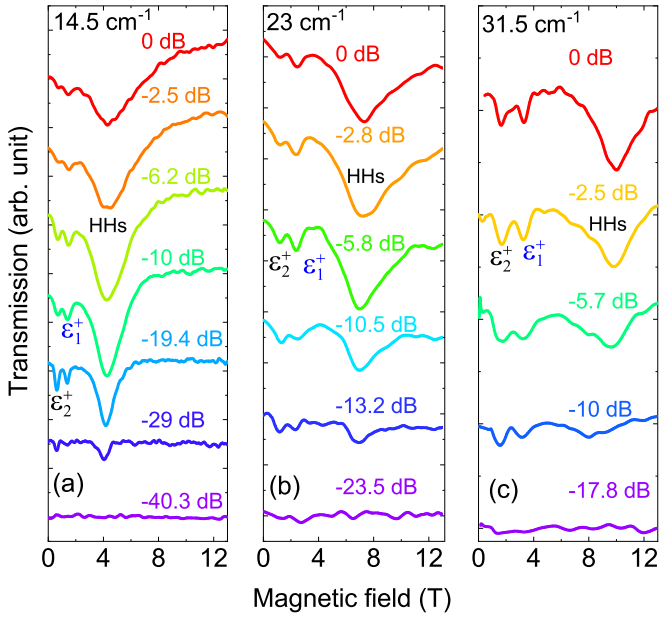

FIG. 6. Intensity-dependent transmission curves as a function of magnetic field, obtained using the FEL frequencies 14.5 (a), 23 (b), and 31.5 (c) cm^{-1} at 4.8 K with the 60 MHz mode. The corresponding peak micropulse intensities near the sample at 0 dB are 7.2, 3.2, and 2.1×10^5 W/cm^2. The different curves are vertically offset for visibility.

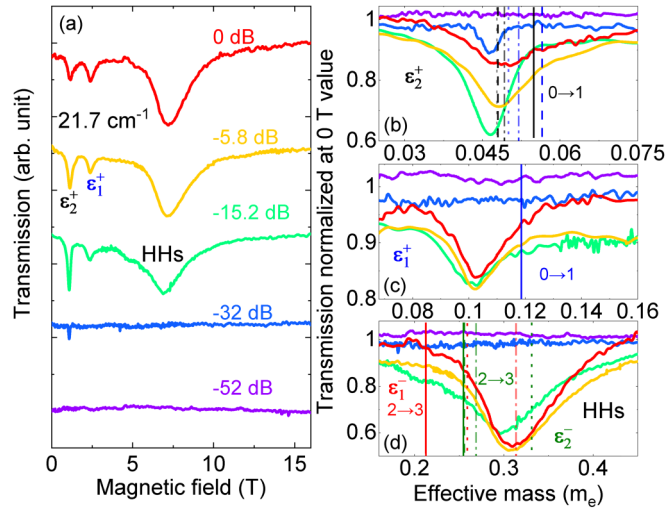

FIG. 7. (a) Intensity-dependent transmission traces as a function of magnetic field at 1.4 K, using a frequency of 21.7 cm^{-1}(3 GHz mode). The micropulse peak intensity was 4.8×10^4 W/cm^2 at 0 dB. A vertical offset was added to each curve for better visibility. (b)–(d) Intensity dependence of the resonance curves for each individual hole subband, where the x-axis is converted to the calculated effective masses using the CR condition. The amplitude values shown correspond to the resonance intensity normalized to the 0 T value. Solid lines indicate the effective masses of the lowest energy transition for each subband (the numbers label the LL transition indices) using the theory of Ref. [34]. The dotted, dashed, and dash-dotted lines mark the higher-order LL transitions. For $\epsilon^+_{1,2}$ these are $1 \to 2$, $2 \to 3$, $3 \to 4$ and for $\epsilon^-_{1,2}$ they are $3 \to 4$, $4 \to 5$, $5 \to 6$, respectively. The same notation is used in Figs. 8 and 9.

drastically increases with power, becomes broader, and finally also saturates at the highest powers. In addition, the peak positions shift as a function of FEL intensity. The CR spectra obtained using the FEL frequencies 23 and 31.5 cm^{-1} exhibit a similar intensity dependence, as shown in Figs. 6(b) and 6(c). This behavior is also recognizable in the experiments using the 3 GHz FEL mode, shown in Figs. 7 and 8. At the lowest radiation power (purple lines in Figs. 7 and 8), no peaks are visible due to the absence of free holes. With increasing FEL power, several peaks subsequently appear and some of them reach saturation. As before, we attribute these peaks to the CR transitions of free holes in the ϵ_2^+, ϵ_1^+, ϵ_1^-, and ϵ_2^- subbands. Figures 7(b)–7(d) and Figs. 8(b)–8(d) show the FEL intensity dependence of the different peaks together with the calculated resonance positions, using Evtuhov's theory [34]. In these plots, the x-axis is converted to effective mass based on the cyclotron resonance condition $\hbar\omega_c = eB/m^*$. The data obtained at 36.0 cm^{-1} reveal very rich behavior. First, at low FEL power (−15.2 dB) the four basic light- and heavy-hole CR transitions appear. The relative amplitudes evolve as a function of the FEL intensity, and most remarkably at intermediate power (−5.2 dB) the two lowest-energy HH transitions saturate and a broad transmission peak appears at higher field strengths, comparable to the broad HH resonance observed in Fig. 6(c). Figure 9 summarizes the results of the CR magnetotransmission study. It shows the energies of the inter-LL transitions of the different subbands and some of the internal Ga dopant transitions as a function of magnetic field up to 30 T. The data points shown by black circles are obtained using FTIR spectroscopy at 20 K, and the red (blue) circles show the data obtained using the 60 MHz (3 GHz) mode of FLARE. The straight lines are calculated by the model discussed in the next section.

III. DISCUSSION

A. Model and calculations

The valence-band edge (at zero momentum $k_z = 0$) consists of six energy levels [32,52], which are split due to the strong spin-orbit coupling. This results in two levels, one of which is fourfold degenerate and the other is twofold degenerate. The twofold degenerate level, called the split-off band, has a total angular momentum $J = \frac{1}{2}$ and is located 290 meV above the bottom of the valence band (not shown in Fig. 1). The fourfold degenerate level has total angular momentum $J = \frac{3}{2}$ and consists of two HH subbands $\epsilon^-_{1,2}$ and two LH subbands $\epsilon^+_{1,2}$. Since the energy difference between the split-off and LH-HH bands is very large, at low temperatures only the LH and HH bands contribute to the optical transitions in the THz range. Hence, in our discussion we restrict ourselves to the behavior of the LH and HH subbands. These subbands interact, resulting in bands that are strongly nonparabolic and give rise to nonequidistant LLs under the application of an external magnetic field, which was studied extensively in the 1950s–1960s, both experimentally and theoretically [33,52]. Wallis and Bowlden [32] specified the theory of CR for the valence band of germanium, which was further developed by Evtuhov [34]. This work took into account the

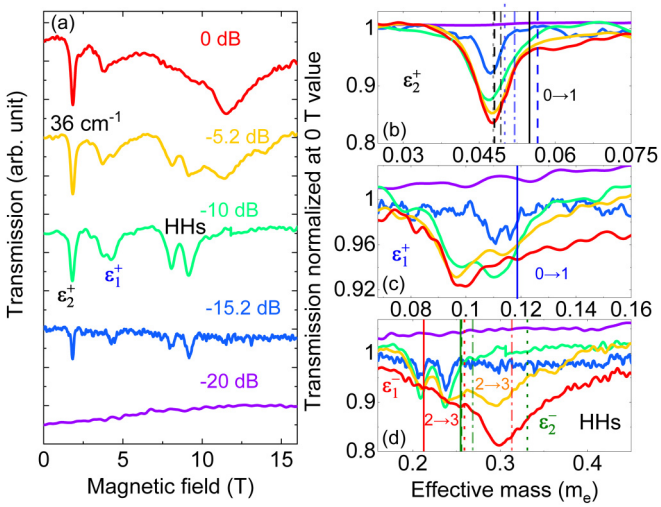

FIG. 8. (a) Intensity-dependent transmission traces as a function of magnetic field at 1.4 K using a FEL frequency of 36 cm^{-1} (3 GHz mode). The micropulse peak intensity was 9.4×10^4 W/cm^2 at 0 dB. A vertical offset was added to each curve for better visibility. (b)–(d) Intensity dependence of the resonance curves for each individual hole subband, which are labeled in the same way as in Fig. 7.

anisotropic valence-band structure and paid special attention to the calculation of the hole wave functions, using the full 6×6 Hamilton operator (for the three different valence bands). A second-order $\mathbf{k} \cdot \mathbf{p}$ and first-order spin-orbit perturbation analysis was used, incorporating five constants, the values of which were based on the work of Dresselhaus [40] and Kane [53]. Based on Evtuhov's notation [34], the following constants were used in this calculations: $l = -31.0$, $\mu = -4.3$, $\nu = -32.4$, $\kappa = 3.3$, and $\Delta = 0.29$ eV.

The situation is quite complex because of the interaction between the different valence subbands, leading to strongly nonparabolic subbands and nonequidistant LLs. The most peculiar subband is the ϵ_1^- level, the minimum of which is not at $k_z = 0$ [32] (not shown in Fig. 1). At $k_z = 0$, the band has a local maximum that results in a negative effective mass. The negative effective mass has consequences for the development of lasers and a negative-effective-mass amplifier/generator [54–56]. In CR experiments, the negative effective mass might influence the spectrum when the magnetic field is directed along the propagation direction of the light and when circularly polarized light is used [57]. Since in our experiments we used unpolarized light and the opposite field direction, the effect of the negative mass is not observable. In our analysis, therefore, we restrict ourselves to the CR transitions at $k_z = 0$, resulting in a sequence of CR transitions that can be characterized by the CR effective masses displayed in Table I [34]. We note that the energy difference (i.e., the condition for CR) between the neighboring LLs is almost $\mathbf{k}$-independent, even if the given n-index subband depends strongly on $\mathbf{k}$ [34]. Therefore, we use the $k_z = 0$ approximation, despite the complex ϵ_1^- subband. Later, we discuss the limit of this approximation. For the light-hole subbands ($\epsilon_{1,2}^+$), the cyclotron effective masses associated with the lowest energy CR transitions are given by $0.055m_e$ and $0.119m_e$. With increasing LL index, these effective masses become smaller. For the heavy-hole subbands $\epsilon_{1,2}^-$, the dependence on the LL index is opposite, i.e., the effective masses for the higher index CRs are higher than their values for the lowest energy transition ($0.213m_e$ and $0.255m_e$).

TABLE I. Calculated values of the cyclotron masses describing transitions at $k_z = 0$ between Landau levels with different index n based on the model of Evtuhov [34]. The $\epsilon_{1,2}^+$ transitions are counted from $n = 0$, whereas the $\epsilon_{1,2}^-$ transitions start from $n = 2$, because in that case the lower n indices result in unphysical eigenvalues of the Hamiltonian [32]. The field-dependent CR transition energies using these masses are indicated in Figs. 4, 7–9.

LL transition	Cyclotron mass (m_e)
$\epsilon_2^+ 0 \to 1$	0.055
$\epsilon_2^+ 1 \to 2$	0.048
$\epsilon_2^+ 2 \to 3$	0.048
$\epsilon_2^+ 3 \to 4$	0.049
$\epsilon_1^+ 0 \to 1$	0.119
$\epsilon_1^+ 1 \to 2$	0.056
$\epsilon_1^+ 2 \to 3$	0.050
$\epsilon_1^+ 3 \to 4$	0.052
$\epsilon_1^- 2 \to 3$	0.213
$\epsilon_1^- 3 \to 4$	0.253
$\epsilon_1^- 4 \to 5$	0.259
$\epsilon_1^- 5 \to 6$	0.314
$\epsilon_2^- 2 \to 3$	0.255
$\epsilon_2^- 3 \to 4$	0.256
$\epsilon_2^- 4 \to 5$	0.331
$\epsilon_2^- 5 \to 6$	0.269

B. THz radiation intensity dependence of the CR transitions

The 20 K FTIR data points (black circles in Fig. 4) closely follow the calculated lowest energy CR transitions indicated by the colored solid lines. Our experiments in the limit of low intensity are, therefore, in good agreement with the theoretical calculation. All four expected $\epsilon_{1,2}^{+,-}$ subbands are observable and identified, and under these conditions (20 K, low intensity) higher index LLs of the different valence subbands are barely populated. A fifth line is visible and characterized by a CR effective mass of $0.36m_e$ (pink line). This transition was observed previously [33] but was not present in our calculation. Its detailed origin is still unknown, and it is attributed to details in the complicated valence-band structure.

In general, with increasing THz power the following happens: the total number of free holes increases (due to a more efficient ionization), which leads to an increasing intensity of the observed CR transitions. Once all Ga acceptors are ionized, the increasing power only changes the distribution of the holes among the LLs, populating the higher index LLs. This leads to a decreasing amplitude (i.e., saturation) of the lower index LL transitions, as already observed in other semiconductors [20].

A large part of the data points obtained using the FEL radiation coincides with the lowest LL index transitions (solid

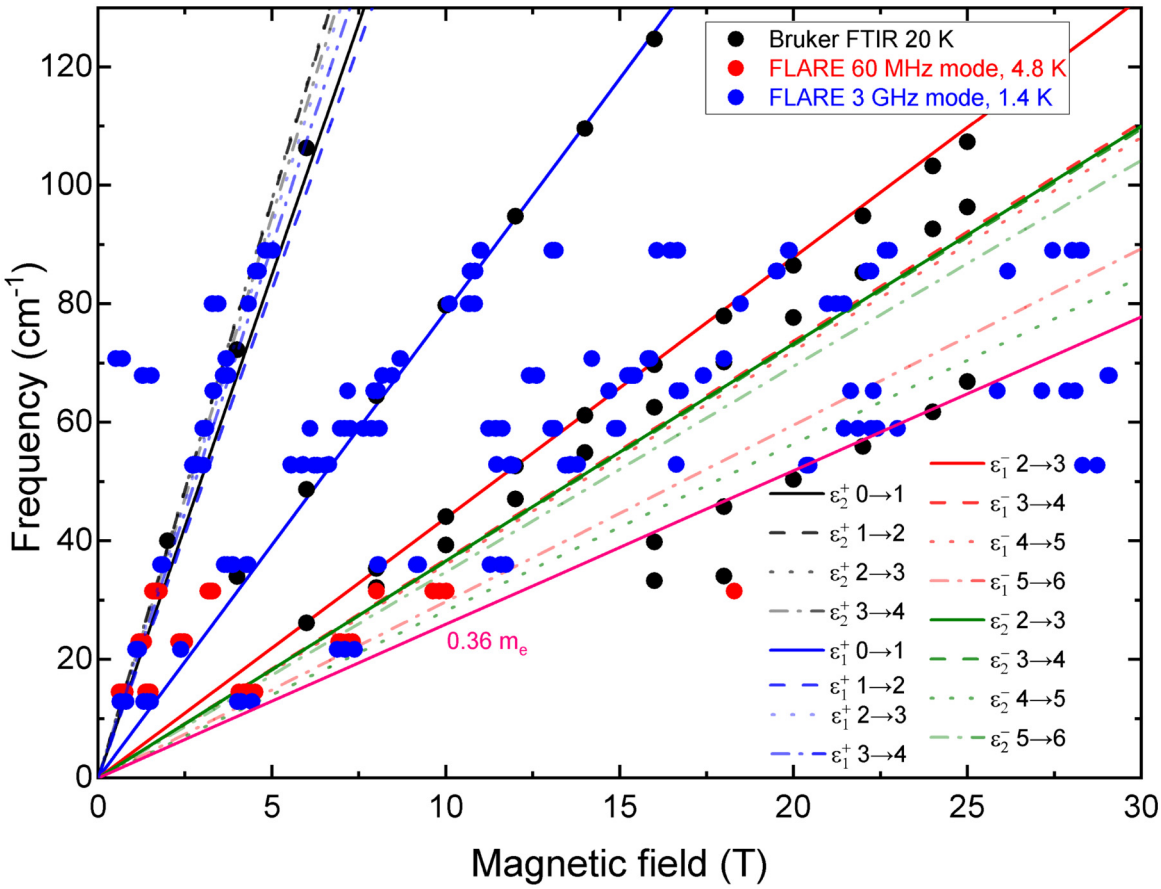

FIG. 9. The frequency-field dependence of the transmission peak energies in Ge:Ga. Black circles correspond to the 20 K FTIR data, and red (blue) circles correspond to the peak positions of all experiments with the 60 MHz (3 GHz) mode of FLARE (all attenuation levels). The 3-GHz mode data points show both CR transitions and internal Ga dopant transitions. The solid lines indicate the calculated behavior of the lowest-energy CR transitions of the different valence hole subbands, and they are the same as the solid lines in Fig. 4 [34]. The dotted, dashed, and dash-dotted lines show the calculated high-order LL transitions [34]. The level indexes are indicated on the plot and are the same as those in Figs. 7 and 8.

lines in Fig. 9). This mainly concerns the results for the low FEL intensities, as well as the data for FEL frequencies above 55 cm^{-1} (3 GHz mode data), i.e., when intracenter Ga transitions facilitate photoionization and the creation of free holes. It is clear though that in this frequency range it is quite difficult to disentangle the CR and intracenter transitions. This problem does not exist for the low FEL frequencies (< 55 cm^{-1}), where we only focus on the radiation intensity dependencies of the amplitude and peak position of the CRs. Remarkably, for the light-hole transitions ($\epsilon^+_{1,2}$) we see relatively narrow CR peaks (see the results in Figs. 6–8). In particular, the ϵ^+_1 CR exhibits a narrow resonance, situated close to the expected position of the $n = 0 \rightarrow n = 1$ transition [Figs. 7(c) and 8(c)]. In fact, the ϵ^+_1 $n = 0 \rightarrow n = 1$ transition is quite isolated in energy (blue solid line in Fig. 9), because the higher index LL ϵ^+_1 transitions are shifted to lower mass values (field values), close to the position of lowest energy ϵ^+_2 CR (black solid line in Fig. 9). Indeed, around this CR peak position [Figs. 7(b) and 8(b)] several ϵ^+_2 and ϵ^+_1 transitions are situated, leading to a nonmonotonic intensity dependence of the CR positions, but still with a rather narrow linewidth. For the HH CR transitions, the situation is different, which is most clearly seen in the traces of the 36 cm^{-1} results using the 3 GHz FEL mode [Fig. 8(d)]. At relatively low FEL intensity (−15.2 and −10 dB), two sharp HH CR dips are detected, the positions of which are close to the calculated lowest energy ϵ^-_1 ($0.213m_e$) and ϵ^-_2 ($0.255m_e$) LL transitions. With increasing intensity (−5.2 and 0 dB) these lines gradually disappear (saturate) and a broad HH resonance is visible at higher field strengths, consistent with the calculated positions of the transitions between the higher index LLs ($\approx 0.3m_e$; see also Fig. 9). Thus, our data directly show the nonequidistant nature of the LLs in the valence band of Ge.

Figure 10 summarizes the effects on the observed CR signal discussed so far, showing the calculated LL energies [34] for the $\epsilon^{+,-}_{1,2}$ subbands in *p*-Ge as a function of the magnetic field at a frequency of 36 cm^{-1}. For this fixed transition energy (shown by the vertical lines), a series of CR transitions are expected. The calculation correctly predicts the positions of the lowest-energy CR transitions of the different subbands, i.e., 2.12 T for ϵ^+_2 (black vertical arrow), 4.57 T for ϵ^+_1 (blue vertical arrow), 8.20 T for ϵ^-_1 (red vertical arrow), and 9.82 T for ϵ^-_2 (green vertical arrow). The higher index LL transitions (indicated by the faded vertical arrows) shift to lower mag-

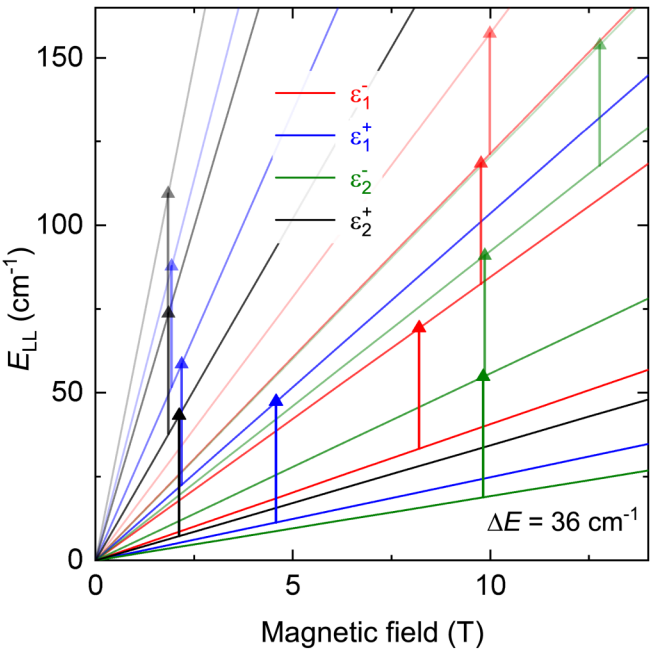

FIG. 10. Calculated Landau level energies for the different valence subbands. Transitions are shown with vertical solid lines for a radiation frequency of 36 cm^{-1} from the lowest LL (solid line) to one level higher (faded line). The vertical lines belong to the higher (more faded) LL transitions.

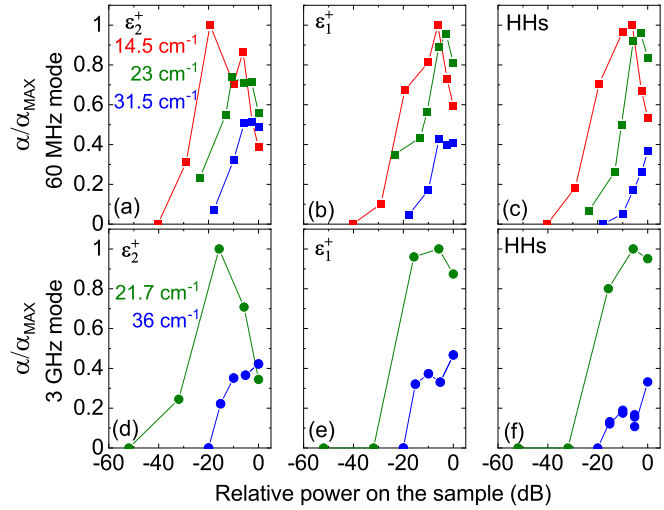

FIG. 11. The power dependence of the relative (normalized to α_{MAX}) absorption coefficients of all the $\epsilon_{1,2}^+$ and the merged HH peaks. (a),(b),(c) are from the 60 MHz mode, while (d),(e),(f) are from the 3 GHz mode. At 36 cm^{-1}, we display all the HH-related peaks without distinction. They are quite close to each other, therefore there are some overlaps among them. The lines between the points are guides for the eye.

netic fields for the LH transitions $\epsilon_{1,2}^+$ and to higher fields for the HH transitions $\epsilon_{1,2}^1$, as observed in the experiment. The experimental conditions obtained with the 3 GHz mode of FLARE at 36 cm^{-1} at 1.4 K are apparently ideal to observe this effect. Free holes are created by photoionization of the Ga centers, and the same FEL light induces inter-Landau-level CR transitions. In this measurement, the effective temperature of the crystal lattice is sufficiently low to keep the linewidth of the CR transitions small enough to see many of the individual transitions and their progression with varying FEL power. Similar behavior is observed for the 21.7 cm^{-1} of 3 GHz mode results and those using the 60 MHz FEL mode. Close inspection of these traces [see, for instance, Figs. 6(c) and 7(d)] shows that the lowest energy CR transitions of the ϵ_1^- ($0.213m_e$) and ϵ_2^- ($0.255m_e$) subbands are weakly visible on the wing of the broader HH resonance at high fields (having a CR effective mass of $\approx 0.3m_e$). Apparently under these conditions, the hole system is already in the high excitation regime at relatively moderate FEL intensities.

This behavior can be partly explained by the fact that at lower magnetic fields the LL spacings are smaller, which makes it both easier to populate higher index LLs and more difficult to resolve individual CR transitions. At the same time, these results suggest that for low FEL frequencies it is easier to ionize the Ga centers. As discussed below, it is quite difficult to compare the results obtained using the different FEL modes. Therefore, we have performed a rough analysis, in which we make a relative comparison of the FEL intensity dependence for each CR transition. Neglecting the field-dependent reflection, we define an absorption coefficient (α) based on the Lambert-Beer law [58] as

$$\alpha = \frac{\ln[T(B=0)/T(B=B_{\rm res})]}{h}, \tag{1}$$

where $T(B=0)$ and $T(B=B_{\rm res})$ are the magnetic-field-dependent transmission values at zero field and at resonance field, and h is the thickness of the sample. $\alpha_{\rm MAX}$ is the largest absorption coefficient for a given transition. Figure 11 shows the relative absorption coefficients against the relative THz power on the sample. First of all, the onset of the CR signals (i.e., the onset of photoionization) for each of the peaks is at lower intensity with decreasing FEL frequency, indicating that photoionization is easier at lower radiation frequency. Second, for each transition the value of the relative absorption coefficient seems to increase with decreasing frequency. Finally, apart from the 36 cm^{-1} excitations and the HH excitation of 31.5 cm^{-1}, the CR transitions show a clear saturation behavior, for which the absorption coefficient increases with growing FEL intensity, reaching a maximum, after which it reduces again.

It is known [59,60] that at resonance, the absorption coefficient does not explicitly depend on the light frequency or the applied magnetic field strength. However, at a given temperature, a higher population difference is desirable to achieve stronger absorption because of the Boltzmann distribution of the holes among the LLs. Therefore, usually no dependence on the magnetic field and light frequency is observed in CR experiments, apart from studies at high temperatures where an increased frequency/field strength results in a stronger absorption and a stronger CR signal. In our low-temperature study, we observe the opposite effect. As discussed in the next

subsection, this might be related to the ionization mechanism being more efficient at the resonance for the lower frequencies, resulting in a significant increase in the population of the initial LL state.

C. Photoionization and Keldysh parameter

THz photoionization studies [36–38] of germanium as a function of magnetic field and doping are still scarce, and we show that it is not straightforward to identify the precise ionization mechanism for all the experiments that we have performed. However, for some experimental conditions we can offer a nonexhaustive explanation using the theory of Keldysh [61,62] and estimate whether we deal with a multiphoton ionization or tunneling effect.

We restrict our discussion to frequencies where direct photoionization is not possible. We limit ourselves to frequencies below the first intracenter Ga transition, i.e., < 55 cm^{-1}, to exclude the contribution of ionization processes via impurity states. Under these conditions, Keldysh theory treats photoionization to be primarily determined by the mean free time of the charge carrier passing through a potential barrier with thickness E_i/qE_ω, where E_ω is the amplitude of the electric component of the radiation and q is the elementary charge. For efficient ionization, the charge carrier has to gain velocity by at least $\sqrt{2E_i/\hat{m}}$ during the radiation period, where $\hat{m} = 10^{-31}$ kg is the mass used for ionization processes [61] in semiconductors. Thus, there is a characteristic threshold frequency

$$\nu_t = \frac{qE_\omega}{2\pi\sqrt{2\hat{m}E_i}}, \tag{2}$$

which describes the timescale of the energy gain of the charged carriers over the thickness of the potential barrier. Using the experimental parameters for gallium-doped germanium, we find that $\nu_t \approx 147$ cm^{-1} for 52.9 cm^{-1} (the highest frequency used below 55 cm^{-1}) and 1128 cm^{-1} for 12.5 cm^{-1}, the lowest frequency used, both in the case of the highest THz laser intensities used. The corresponding Keldysh parameter γ is defined as the ratio of the radiation frequency and the threshold frequency, leading to $\gamma = 0.01$ and 0.36 for 12.5 and 52.9 cm^{-1}, respectively. Since the criterion for multiphoton ionization is $\gamma \gg 1$, we claim that we are in the opposite limit, where the field-ionization (i.e., tunnel effect) is dominant, in agreement with a previous study [38]. On the other hand, for low-power radiation at intermediate frequencies, we can reach values of $\gamma > 30$, as shown in Table S1 of the Supplemental Material [48]. Thus, there are regions in our parameter space where the multiphoton process has a larger probability.

Qualitatively, we can explain our photoionization results below 55 cm^{-1} as follows. The charge carrier has less time to tunnel through the barrier within one radiation cycle with increasing light frequency. As a result, the tunneling probability reduces with increasing frequency, as seen in Fig. 11. However, the multiphoton process becomes more efficient with growing frequency. Distinguishing these two effects requires measuring the frequency dependence of the ionization efficiency at frequencies above the characteristic frequency ν_t, but below the energies of single-photon ionization, which is a relatively narrow range for Ge:Ga, as indicated above. We note that a more realistic description of the process is more complicated and should involve the finite temperature of the experiment, the effect of the magnetic field, and the doping dependence of the ionization. Nevertheless, we believe that further ionization studies of Ge:Ga would contribute to developing broad-range, fast THz detectors.

D. Future challenges

Many observations in our experiment can be reasonably described and explained by the band-structure and photoionization theories introduced above. A full quantitative understanding is, however, quite difficult to obtain, due to the inherent complexity of the valence band of Ge and due to the lack of temporal information.

First of all, we have restricted our analysis to the calculated behavior of the valence hole subbands at $k_z = 0$ and the corresponding power related changes in the spectra. This is clearly a simplification, evidenced by the observation of the fifth CR line characterized by a CR effective mass of $0.36m_e$ [33] and the appearance of additional transmission peaks even below this fifth transition [see two FTIR data points (black circles) and one FEL data point (red circle) in Fig. 9]. In this range, there are no Ga intracenter transitions and LL transitions with a selection rule of $\Delta n = \pm 1$. We believe that these points might originate from different selection rules of the CR as discussed in Ref. [33]. A second issue regards the whole subband curvature in the Brillouin zone: based on the theory, towards high magnetic fields the effective mass should increase, though this effect is fairly small [34]. A third issue is the simultaneous occurrence of photoionization of the Ga dopants and CR transitions. The ionization is a nonresonant process that creates free holes that distribute themselves over the different subbands. This process is most probably field- (and frequency-) dependent, also because of the occurrence of CR and the effect of screening of the dopant charges by the free holes. This affects the overall refractive index of the sample as a function of field strength and radiation power.

Finally, the distinct FEL modes of operation might also play an important role considering the dynamics of the valence-band states, because the 60 MHz and 3 GHz modes of FLARE have a difference in spectral resolution and average power (see the Supplemental Material [48]). Time-resolved studies of the valence-band transitions in germanium [3,63] resulted in a measured capture time of free holes by the dopant states (i.e., the depletion time of the valence band after photoionization) in the range of 1–20 ns, depending on the occupation of the band. Using the 60 MHz mode (with a time separation of 16.67 ns between the micropulses), the FEL micropulses create free holes, which are able to relax back to the Ga centers in between the micropulses in most cases, making the effect of all micropulses similar. Instead, in the 3 GHz mode, with a micropulse time-separation of only 0.33 ns, the first micropulse generates free carriers that do not relax back to the dopant centers before the next micropulse arrives. Therefore, the consecutive micropulses are incident on a sample already containing free carriers. The different modes of operation thus might affect the time-averaged results obtained in this study.

Therefore, the full explanation of the amplitude and linewidth behavior of the CR transitions as a function of the FEL intensity requires us to obtain precise information and control on the carrier concentration in the band. Complementary techniques such as photoconductivity, transmission with reference, or time-resolved measurements might be very helpful for further studies.

IV. CONCLUSIONS

In conclusion, we have reported the THz magnetotransmission spectra of gallium-doped germanium employing low-power FTIR and high-power FEL radiation. We showed that intense, pulsed THz radiation with frequencies below the Ga ionization energy (89 cm^{-1}) can effectively ionize the Ga centers creating free holes in the valence bands, leading to ideal conditions for a detailed CR study of the valence band in Ge. For photon energies above the lowest-energy internal Ga transition (55 cm^{-1}), intradopant transitions are simultaneously observed with narrow CR peaks. The internal Ga transitions have been characterized using FTIR spectroscopy, and they exhibit both linear and quadratic Zeeman terms. For energies below 55 cm^{-1}, only CR transitions have been observed with amplitudes and peak positions that strongly depend on the THz radiation intensity. At low and moderate radiation intensities (both FTIR at 20 K and FEL), we identify all four lowest-energy Landau level transitions of the HH and LH subbands, the positions of which are in good agreement with effective-mass theory of the Ge valence band taking into account transitions at the center of the Brillouin zone (at $k_z = 0$). The appearance of these lowest-energy CR peaks marks the onset of photoionization, which is found to be more efficient for lower FEL frequencies. Quantifying the Keldysh parameter in this regime, we estimate that under these experimental conditions, the field ionization is dominant. With increasing FEL intensity, complex behavior of the CR signals is seen, which is related to the complicated valence-band structure. We observed that the heavy- (light-) hole CR peaks mostly shift to higher (lower) magnetic field with increasing radiation intensity, which is also consistent with the theoretical calculations for the $k_z = 0$ transitions. Our studies also reveal CR transitions that cannot be explained by the theory we used, such as a transition with a CR effective mass of $0.36m_e$ and some peaks with a mass that is even heavier. Our time-averaged studies of these nonlinear magneto-optical processes in gallium-doped germanium using a pulsed free-electron laser might be very relevant for developing THz lasers, photonics, and detectors. However, it is obvious that a full explanation of the nonlinear CR properties requires more experimental and theoretical investigations.

Overall, our saturation spectroscopy technique unprecedentedly expands the parameter space of the magnetic field, THz frequency, and intensity, offering an exciting perspective for the research of semiconductors, especially 2DEGs, where the carrier concentration can be kept constant over a wide range of THz intensity.

ACKNOWLEDGMENTS

This work was supported by HFML-RU/NWO, a member of the European Magnetic Field Laboratory (EMFL). This work is part of the research program of the Netherlands Organisation for Scientific Research (NWO). The authors thank Alexander van der Meer for useful discussions. B.B. acknowledges support by the European Research Council (Grant Agreement No. 835279-Catch-22).

[1] D. Seo, J. M. Gregory, L. C. Feldman, N. H. Tolk, and P. I. Cohen, Multiphoton absorption in germanium using pulsed infrared free-electron laser radiation, Phys. Rev. B **83**, 195203 (2011).

[2] M. A. W. van Loon, N. Stavrias, N. H. Le, K. L. Litvinenko, P. T. Greenland, C. R. Pidgeon, K. Saeedi, B. Redlich, G. Aeppli, and B. N. Murdin, Giant multiphoton absorption for THz resonances in silicon hydrogenic donors, Nat. Photon. **12**, 179 (2018).

[3] N. Deßmann, S. Pavlov, V. Tsyplenkov, E. Orlova, A. Pohl, V. Shastin, R. K. Zhukavin, S. Winnerl, M. Mittendorff, J. Klopf *et al.*, Dynamics of non-equilibrium charge carriers in p-germanium doped by gallium, Phys. Status Solidi B **254**, 1600803 (2017).

[4] W. Wang, L. Xu, X. Wei, and S. Zhang, Intense-terahertz-laser modulated photoionization cross section of shallow-donor impurity in semiconductors in a magnetic field, Results Phys. **20**, 103692 (2021).

[5] M. Seo, J.-H. Kang, H.-S. Kim, J. H. Cho, J. Choi, Y. M. Jhon, S. Lee, J. H. Kim, T. Lee, Q.-H. Park *et al.*, Observation of terahertz-radiation-induced ionization in a single nano island, Sci. Rep. **5**, 7969 (2015).

[6] W. Heiss, P. Auer, E. Gornik, C. R. Pidgeon, C. J. G. M. Langerak, B. N. Murdin, G. Weimann, and M. Heiblum, Determination of Landau level lifetimes in AlGaAs/GaAs heterostructures with a ps free electron laser, Appl. Phys. Lett. **67**, 1110 (1995).

[7] S. K. Singh, B. D. McCombe, J. Kono, S. J. Allen, Jr., I. Lo, W. C. Mitchel, and C. E. Stutz, Saturation spectroscopy and electronic-state lifetimes in a magnetic field in I n A s/A l x Ga 1- x Sb single quantum wells, Phys. Rev. B **58**, 7286 (1998).

[8] M. Forcales, M. Klik, N. Q. Vinh, I. V. Bradley, J.-P. R. Wells, and T. Gregorkiewicz, Free-electron laser studies of energy transfer mechanisms in semiconductors doped with transition series ions, J. Lumin. **94-95**, 243 (2001).

[9] G. R. Allan, A. Black, C. R. Pidgeon, E. Gornik, W. Seidenbusch, and P. Colter, Impurity and Landau-level electron lifetimes in *n*-type GaAs, Phys. Rev. B **31**, 3560 (1985).

[10] T. Winzer, A. Knorr, M. Mittendorff, S. Winnerl, M.-B. Lien, D. Sun, T. B. Norris, M. Helm, and E. Malic, Absorption saturation in optically excited graphene, Appl. Phys. Lett. **101**, 221115 (2012).

[11] B. N. Murdin, W. Heiss, C. J. G. M Langerak, S.-C. Lee, I. Galbraith, G. Strasser, E. Gornik, M. Helm, and C. R. Pidgeon,

Direct observation of the lo phonon bottleneck in wide GaAs/Al x Ga 1- x As quantum wells, Phys. Rev. B **55**, 5171 (1997).

[12] B. Cole, J. Williams, B. King, M. Sherwin, and C. Stanley, Coherent manipulation of semiconductor quantum bits with terahertz radiation, Nature (London) **410**, 60 (2001).

[13] P. Greenland, S. A. Lynch, A. Van der Meer, B. Murdin, C. Pidgeon, B. Redlich, N. Vinh, and G. Aeppli, Coherent control of Rydberg states in silicon, Nature (London) **465**, 1057 (2010).

[14] S. Chick, N. Stavrias, K. Saeedi, B. Redlich, P. Greenland, G. Matmon, M. Naftaly, C. Pidgeon, G. Aeppli, and B. N. Murdin, Coherent superpositions of three states for phosphorous donors in silicon prepared using THz radiation, Nat. Commun. **8**, 16038 (2017).

[15] S. Takahashi, L.-C. Brunel, D. Edwards, J. Van Tol, G. Ramian, S. Han, and M. Sherwin, Pulsed electron paramagnetic resonance spectroscopy powered by a free-electron laser, Nature (London) **489**, 409 (2012).

[16] C. B. Wilson, D. T. Edwards, J. A. Clayton, S. Han, and M. S. Sherwin, Dressed Rabi Oscillation in a Crystalline Organic Radical, Phys. Rev. Lett. **124**, 047201 (2020).

[17] M. Ozerov, B. Bernáth, D. Kamenskyi, B. Redlich, A. van der Meer, P. C. M. Christianen, H. Engelkamp, and J. C. Maan, A THz spectrometer combining the free electron laser FLARE with 33 T magnetic fields, Appl. Phys. Lett. **110**, 094106 (2017).

[18] S. Zvyagin, M. Ozerov, E. Čižmár, D. Kamenskyi, S. Zherlitsyn, T. Herrmannsdörfer, J. Wosnitza, R. Wünsch, and W. Seidel, Terahertz-range free-electron laser electron spin resonance spectroscopy: Techniques and applications in high magnetic fields, Rev. Sci. Instrum. **80**, 073102 (2009).

[19] M. Ozerov, J. Romhanyi, M. Belesi, H. Berger, J.-P. Ansermet, J. van den Brink, J. Wosnitza, S. A. Zvyagin, and I. Rousochatzakis, Establishing the Fundamental Magnetic Interactions in the Chiral Skyrmionic Mott Insulator Cu_2OSeO_3 by Terahertz Electron Spin Resonance, Phys. Rev. Lett. **113**, 157205 (2014).

[20] E. Gornik, T. Y. Chang, T. J. Bridges, V. T. Nguyen, J. D. McGee, and W. Müller, Landau-Level-Electron Lifetimes in n-InSb, Phys. Rev. Lett. **40**, 1151 (1978).

[21] B. Murdin, M. Kamal-Saadi, C. Ciesla, C. Pidgeon, C. Langerak, R. Stradling, and E. Gornik, Landau level lifetimes in an InAs/AlSb quantum well determined by a picosecond far-infrared pump-probe technique, Physica Status Solidi B **204**, 155 (1997).

[22] M. Mittendorff, F. Wendler, E. Malic, A. Knorr, M. Orlita, M. Potemski, C. Berger, W. A. De Heer, H. Schneider, M. Helm *et al.*, Carrier dynamics in Landau-quantized graphene featuring strong Auger scattering, Nat. Phys. **11**, 75 (2015).

[23] R. E. Camacho-Aguilera, Y. Cai, N. Patel, J. T. Bessette, M. Romagnoli, L. C. Kimerling, and J. Michel, An electrically pumped germanium laser, Opt. Express **20**, 11316 (2012).

[24] K. Unterrainer, C. Kremser, E. Gornik, C. R. Pidgeon, Y. L. Ivanov, and E. E. Haller, Tunable Cyclotron-resonance Laser in Germanium, Phys. Rev. Lett. **64**, 2277 (1990).

[25] N. H. Le, G. V. Lanskii, G. Aeppli, and B. N. Murdin, Giant non-linear susceptibility of hydrogenic donors in silicon and germanium, Light Sci. Appl. **8**, 64 (2019).

[26] A. Mayer and F. Keilmann, Far-infrared nonlinear optics. II. χ (3) contributions from the dynamics of free carriers in semiconductors, Phys. Rev. B **33**, 6962 (1986).

[27] P. R. Bratt, Impurity germanium and silicon infrared detectors, in *Semiconductors and Semimetals* (Elsevier, Amsterdam, 1977), Vol. 12, pp. 39–142.

[28] G. Wang, M. Zhang, Y. Zhu, G. Ding, D. Jiang, Q. Guo, S. Liu, X. Xie, P. K. Chu, Z. Di *et al.*, Direct growth of graphene film on germanium substrate, Sci. Rep. **3**, 3427 (2013).

[29] N. Miura, *Physics of Semiconductors in High Magnetic Fields* (Oxford University Press, Oxford, 2008), Vol. 15.

[30] K. Suzuki and N. Miura, Quantum cyclotron resonance in GaSb and Ge in high magnetic fields up to 330 kG, J. Phys. Soc. Jpn. **39**, 148 (1975).

[31] D. Molter, F. Ellrich, T. Weinland, S. George, M. Goiran, F. Keilmann, R. Beigang, and J. Léotin, High-speed terahertz time-domain spectroscopy of cyclotron resonance in pulsed magnetic field, Opt. Express **18**, 26163 (2010).

[32] R. Wallis and H. Bowlden, Theory of the valence band structure of germanium in an external magnetic field, Phys. Rev. **118**, 456 (1960).

[33] J. Stickler, H. Zeiger, and G. Heller, Quantum effects in Ge and Si. I, Phys. Rev. **127**, 1077 (1962).

[34] V. Evtuhov, Valence bands of germanium and silicon in an external magnetic field, Phys. Rev. **125**, 1869 (1962).

[35] B. Lax and J. G. Mavroides, Cyclotron resonance, in *Solid State Physics*, edited by F. Seitz and D. Turnbull (Elsevier, Lexington, 1960), Vol. 11, pp. 261–400.

[36] B. Lax and D. Cohn, Interaction of intense submillimeter radiation with plasmas, IEEE Trans. Microwave Theory Tech. **22**, 1049 (1974).

[37] M. Leung and H. Drew, Nonlinear far-infrared photoconductivity in Ge:Ga, Appl. Phys. Lett. **45**, 675 (1984).

[38] Y. Mukai, H. Hirori, and K. Tanaka, Electric field ionization of gallium acceptors in germanium induced by single-cycle terahertz pulses, Phys. Rev. B **87**, 201202(R) (2013).

[39] S. Ganichev, W. Prettl, and I. Yassievich, Deep impurity-center ionization by far-infrared radiation, Phys. Solid State **39**, 1703 (1997).

[40] G. Dresselhaus, A. Kip, and C. Kittel, Cyclotron resonance of electrons and holes in silicon and germanium crystals, Phys. Rev. **98**, 368 (1955).

[41] R. Dexter, H. Zeiger, and B. Lax, Anisotropy of cyclotron resonance of holes in germanium, Phys. Rev. **95**, 557 (1954).

[42] R. Fletcher, W. Yager, and F. Merritt, Observation of quantum effects in cyclotron resonance, Phys. Rev. **100**, 747 (1955).

[43] C. Bradley, K. Button, B. Lax, and L. Rubin, Quantum effects in cyclotron resonance using a CW hydrogen-cyanide laser, IEEE J. Quantum Electron. **4**, 733 (1968).

[44] R. Dexter, H. Zeiger, and B. Lax, Cyclotron resonance experiments in silicon and germanium, Phys. Rev. **104**, 637 (1956).

[45] S. Wiegers, P. Christianen, H. Engelkamp, A. den Ouden, J. Perenboom, U. Zeitler, and J. Maan, The high field magnet laboratory at Radboud University Nijmegen, J. Low Temp. Phys. **159**, 389 (2010).

[46] R. Johnson and P. Kuby, *Elementary Statistics, Enhanced Review Edition* (Cengage Learning, Belmont, 2007).

[47] D. Cuttriss, Relation between surface concentration and average conductivity in diffused layers in germanium, Bell Syst. Tech. J. **40**, 509 (1961).

[48] See Supplemental Material at http://link.aps.org/supplemental/10.1103/PhysRevB.105.205204 for the details.

[49] R. L. Jones and P. Fisher, Excitation spectra of group III impurities in germanium, J. Phys. Chem. Solids **26**, 1125 (1965).

[50] R. E. M. Vickers, R. A. Lewis, P. Fisher, and Y.-J. Wang, Terahertz Zeeman spectroscopy of boron in germanium to high magnetic fields, Phys. Rev. B **77**, 115212 (2008).

[51] We assume $\sigma = 0.5\text{cm}^{-1}$ standard deviation on the THz light, and we take 0.5% uncertainty for the magnetic field values. We also note that these error bars are taken into account in the size of the circles in Figs. 4 and 9.

[52] J. M. Luttinger, Quantum theory of cyclotron resonance in semiconductors: General theory, Phys. Rev. **102**, 1030 (1956).

[53] E. O. Kane, Energy band structure in p-type germanium and silicon, J. Phys. Chem. Solids **1**, 82 (1956).

[54] A. A. Andronov, A. M. Belyantsev, V. I. Gavrilenko, E. P. Dodin, E. F. Krasil'nik, V. V. Nikonorov, S. A. Pavlov, and M. M. Shvarts, Germanium hot-hole cyclotron-resonance maser with negative effective hole masses, Zh. Eksp. Teor. Fiz. **90**, 367 (1986) [Sov. Phys.-JETP **63**, 211 (1986)].

[55] A. Andronov, A. Beliantsev, V. Gavrilenko, E. Dodin, Z. Krasilnik, V. Nikonorov, and S. Pavlov, Induced hot-hole millimeter emission in germanium in fields E‖H (cyclotron-resonance negative-effective-mass amplifier and generator), Zh. Eksp. Teor. Fiz. Pis'ma Redakt. **40**, 221 (1984).

[56] A. Zakharov, Instability in a semiconductor amplifier with negative effective carrier mass, Zh. Eksp. Teor. Fiz. **38**, 665 (1960).

[57] G. Dousmanis, R. Duncan, Jr., J. Thomas, and R. Williams, Experimental Evidence for Carriers with Negative Mass, Phys. Rev. Lett. **1**, 404 (1958).

[58] F. Demichelis, G. Kaniadakis, A. Tagliaferro, and E. Tresso, New approach to optical analysis of absorbing thin solid films, Appl. Opt. **26**, 1737 (1987).

[59] H. J. A. Bluyssen, J. C. Maan, T. B. Tan, and P. Wyder, Study of cyclotron-resonance-induced conductivity in n-GaAs, Phys. Rev. B **22**, 749 (1980).

[60] K. Kobayashi and E. Otsuka, Cyclotron resonance of hot electrons and nonlinear transport phenomena in n-type indium antimonide, J. Phys. Chem. Solids **35**, 839 (1974).

[61] L. Keldysh, Ionization in the field of a strong electromagnetic wave, Sov. Phys. JETP **20**, 1307 (1965).

[62] A. M. Zheltikov, Keldysh parameter, photoionization adiabaticity, and the tunneling time, Phys. Rev. A **94**, 043412 (2016).

[63] B. Bernáth, FEL-based THz spectroscopy in high magnetic fields, Ph.D. thesis, Radboud University, 2021.